# Dynamics of Dust and Gas in Debris Discs

Thomas Baycroft
Christ's College, University of Cambridge

4th of May 2021

**Abstract**

Many stars have dusty remnants surrounding them called debris discs. Some debris discs have been found to have gas, with a few also having complex structure such as multiple dust rings. The origin of this gas (Primordial or Secondary) is debated, and may in fact be different in different discs. This may also place these discs in different places along their evolutionary track. Debris discs are optically thin so the effect of radiation pressure from the star on small dust is significant. Rocky planetesimal belts can, through collisions, release dust and gas into a disc.
In this project we model the injection of dust and gas into a gas disc, and the effect that radiation pressure has on the dynamics of these. We include the back-reaction of the dust on the gas, which has so far mostly been omitted, this back-reaction can be highly important in cases with low gas content. We present various results from 1-D axisymmetric simulations of a disc. We use these to describe an evolutionary mechanism that these discs could follow, doing this across a range of viscosities, also changing other parameters such as gas content and number of dust species. This evolutionary mechanism is the start of a pathway to explaining structures seen in these discs. We find a possible way of determining whether the gas in such a system is primordial or second generation.

# 1 Introduction

## 1.1 Circumstellar Discs

The study of Circumstellar Discs is a young and very active area of research. Characteristics of Circumstellar discs vary greatly, for example radial extent, gas and dust content, and structures such as gaps or rings. Various different aspects of these discs have been studied, many of which are not yet properly understood.

Circumstellar discs can be divided into 3 categories: protoplanetary discs which are young, and debris discs which are old, and transition discs in between [Williams and Cieza, 2011].

Protoplanetary discs contain a lot of gas and they will usually have a very small amount of dust in proportion to the gas. Debris discs have a large amount of dust and usually very little gas [Zuckerman et al., 1995]. The dust is thought to have been formed by collisions between planets or planetesimals [Wyatt, 2008]. These discs are analogous to the Kuiper and asteroid belts in our own Solar system, except with a much larger amount of dust (otherwise we would not be able to

observe them). By this stage in the disc's evolution, the vast majority of the gas is expected to have disappeared by accretion onto the star, photoevaporation, or some other mechanism [Williams and Cieza, 2011, Fedele et al., 2010] .

A few debris discs do still have significant gas content[Dent et al., 2005][Moór et al., 2011], a notable example being $\beta$-Pic [Dent et al., 2014], these are often referred to as Hybrid discs.

## 1.2 Hybrid Discs

Hybrid discs are rare and not very well understood, a few main ones in addition to $\beta$-Pic are: 49-Ceti [Zuckerman et al., 1995, Moór et al., 2011], HD21997 [Kóspál et al., 2013], and HD 141569 [Dent et al., 2005, Di Folco et al., 2020]. Gas in debris discs is hard to detect, so as advances in telescopes are making detecting this gas easier, many more Hybrid discs are likely to be identified. The study of gas content in debris discs is therefore a developing area, and understanding the relative dynamics of the gas and dust is key to the future development of the field.

Dust in debris discs can be released from collisional cascades [Wyatt, 2008], effectively resulting in a steady release of small dust from a planetesimal belt. We will be implementing this idea in our modelling by simply inputting small dust in a given region.

Similarly, gas may be released from a planetesimal belt, CO gas can be frozen or trapped in ice. Various mechanisms for the release of this gas have been theorised, such as photodesorption or collisional vaporisation of icy grains [Hughes et al., 2018]. We will be modelling this by inputting gas, usually over the same region as the dust, since it is the planetesimal belt which would give rise to both.

The origin of the gas in hybrid discs is debated, whether it is some long lived primordial gas or a second generation gas that has been released [Hughes et al., 2018]. Arguments against primordial gas are that these discs are older than the accepted gas-accretion timescales [Fedele et al., 2010], and without some strong shielding from the stellar UV flux, the CO gas should have been destroyed [Moór et al., 2011], additionally, models are not able to reproduce the chemical composition of the gas seen in sub-mm emission [Roberge et al., 2013]. Arguments against secondary sources are that an extremely high rate of creation of CO gas would be required for gas seen to be in steady state (as CO should have a very short lifetime) [Moór et al., 2011] and that if gas and dust are not co-located it is less plausible for them to have been produced in the same parent belt, unless some mechanism causes them to evolve differently [Kóspál et al., 2013].

One possible resolution to this is that for gas being released, if not in steady state, the discs could simply be in a short-lived state of very high gas production [Roberge et al., 2013, Moór et al., 2011]. Another possibility is that the CO gas which has a very short lifetime is being shielded by C gas [Kral et al., 2019].

Most of the investigations into the origin of this gas deal with the photochemistry and gas lifetime, a few consider dynamical effects, in particular, the relation to the dust. Even fewer so far have included the back-reaction of the dust onto the gas as we will do. We therefore investigate whether looking at the dust-gas dynamics can give a different method of establishing the origin of the gas in hybrid systems.

Some of these Hybrid discs have a complex structure. A good example of this is HD 141569 which has various dust rings in sub-$\mu$m grains, as shown in Figure 1 [Di Folco et al., 2020]. The dynamics at play in these Hybrid discs are not well understood, in particular those which could account for this kind of structure.

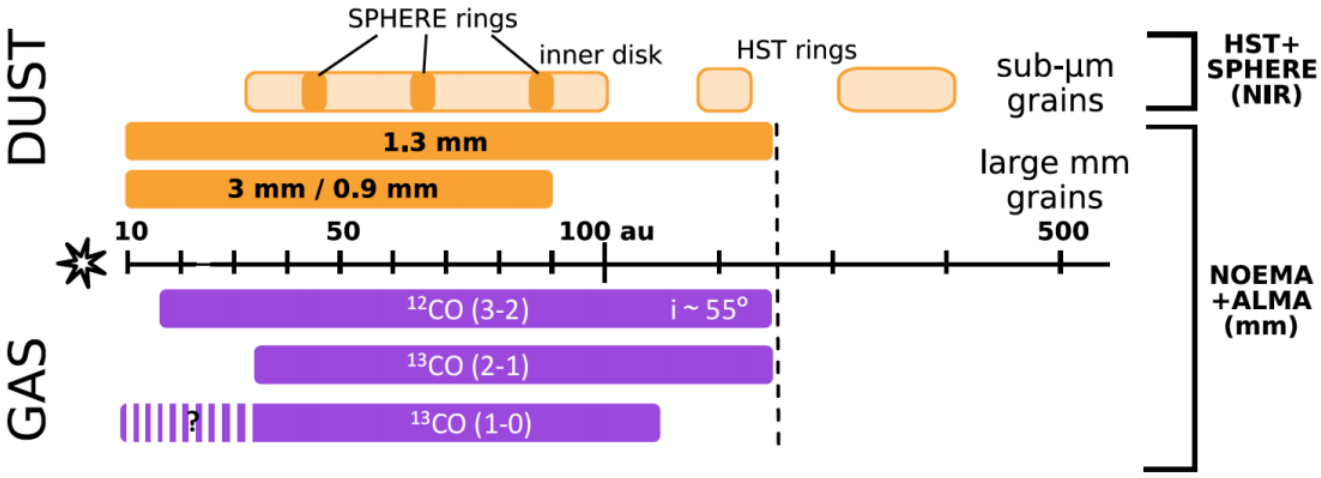


Figure 1: Structure of HD 141569 as described in [Di Folco et al., 2020]

One of the aims of this project is, in investigating the dynamics involved, to lay a foundation for future work to develop, with a view of understanding how these hybrid discs have come to be, and why they exhibit the structure they do.

## 1.3 Dust-Gas Dynamics

A test particle will follow a circular Keplerian orbit around a star. In reality other forces act on particles which may deviate them from such orbits. A pressure gradient will change the effective potential in which the gas sits. A positive gradient will mean the gas orbits super-keplerian (faster) and a negative gradient will mean it orbits sub-keplerian (slower).

Dust is acted on by radiation pressure from the star, the force acting on the dust depends on the surface area of the grains so smaller dust will experience a stronger force per unit mass. If the dust is small enough the radiation pressure force exceeds gravity, so the dust will simply be blown out on a dynamical timescale. Larger dust than this will have the radiation pressure working against gravity, so it will have a sub-Keplerian orbit. Even larger dust will have a minimal radiation pressure force, so will have close to a Keplerian orbit.

The relative azimuthal velocity of the dust and gas is therefore dependent on both the gas pressure gradient and the dust grain size (via the radiation pressure). If the effect of the radiation pressure is stronger than that of the gas pressure gradient, then the dust will orbit slower than the gas. Once drag is included, angular momentum will be transferred from the gas to the dust, the result will be the dust moving outwards and the gas moving inwards. If the radiation pressure is weaker than the gas gradient the opposite will be true [Marino et al., 2020].

In addition to this, the dust will be subject to diffusion, and the gas to viscous diffusion, these will act to damp out strong gradients in the dust-to-gas ratio.

Hybrid discs and, more generally, Debris discs are usually optically thin [Hughes et al., 2018], so the radiation pressure from the central star on the dust is important throughout the radial extent of the disc.

There have been a few dynamical studies of hybrid discs. [Takeuchi and Artymowicz, 2001] looked at the effect of radiation pressure on dust in a gaseous disc, finding that it can migrate inwards or outwards depending on dust size (as described above), and that small dust will drift outwards up to the edge of the gas disc, where the drop-off in density can cause the dust to accumulate into a ring. Observations of HD 141569A and HR 4796A are used for a qualitative comparison. [Kral et al., 2016] investigated C and O being released from the photodissociation of CO in $\beta$-Pic and the viscous evolution of this gas, the dust is only included through its effect on the temperature, the dynamical effects being ignored. Observations of [CI] with APEX [OI] with Hershel as well as [CII] and [CO] are used. [Kral et al., 2019] investigate the shielding of CO by C, and the viscous evolution of this gas, using observations of [CI] in HD 131835 for comparison. [Marino et al., 2020] use this in a population synthesis, and describe the effect on dust.

None of these, however, include the back-reaction of the dust on the gas. In systems with a high dust-to-gas ratio this will be an important effect to consider and might have a large impact on the gas distribution. Models done by [Lyra and Kuchner, 2013] do include the dust back-reaction, but do not include radiation pressure or look at any dust or gas input. They find that narrow eccentric dust rings can form due to a photoelectric instability, and compare this to observations of the Formalhaut debris disc.

In this project we build on previous dynamical studies and include the back-reaction of the dust on the gas (which has not often been included in modelling and can have a large effect in dust-rich discs). We model the input of dust and gas into a pre-existing gas disc and investigate the evolution over a range of values in different parameters. This will shed light onto a possible way that structure in hybrid discs can form, and to a difference in structure between primordial/secondary gas which may lead to a new way of establishing which type of gas a disc has.

# 2 Model Description

For this work, we use a version of the model from [Booth et al., 2017] which solves the viscous evolution, following an $\alpha$ prescription [Shakura and Sunyaev, 1973] for the viscosity, that is, $\nu = \alpha c_s H$, with $\alpha$ a dimensionless parameter, as well as computing the dust-gas drag, and the back-reaction of the dust on the gas (we refer to this as feedback). We use a simplified dust model with fixed dust sizes (hence no dust growth or fragmentation). We simulate using 500 cells equally spaced in $R^{1/2}$ from either 0.1 au or 10 au, up to 1000au.

This model solves the usual viscous evolution equation

$$\frac{d\Sigma}{dt} = \frac{1}{R}\frac{d}{dR}\left(3R^{1/2}\frac{d}{dR}\left[\nu\Sigma_G R^{1/2}\right]\right) \tag{1}$$

Where $\nu$ is the kinematic viscosity for which we use the $\alpha$ prescription above, $\Sigma_G$ is the gas surface density, and $\Sigma$ is the sum of the gas surface density and the individual dust-species surface densities.

The dust velocites are determined by the gas drag, the force for this is

$$F_{drag} = \frac{m\Delta v}{t_s} \tag{2}$$

where $m$ is the dust grain mass, $\Delta v$ the dust-gas relative velocity, and $t_s$ the stopping time which is the time for the gas drag to reduce $\Delta v$ to zero. The dimensionless stopping time, or Stokes' number, is $St = \Omega_k t_s$, where $\Omega_k$ is the keplerian orbital velocity. For small dust particles ($D < 9/2\lambda$, $\lambda$ the gas's mean free path) we are in the Epstein drag regime and the Stokes' number can be characterised as [Birnstiel et al., 2012]:

$$St_i = \frac{\pi \rho_s D_i}{4\Sigma_G} \tag{3}$$

where $\rho_s$ is the internal density of the dust grains and $D_i$ is the grain diameter of the $i$'th species of dust.

The relative dust-gas velocities are

$$\Delta v_i = \frac{2u_\phi St_i - u_r St_i^2}{1 + St_i^2} \tag{4}$$

Where $u_\phi$ and $u_r$ are the azimuthal and radial gas velocities. $St_i$ is the Stokes' number of the $i$'th dust species.

The model also evaluates diffusion of the dust and trace species, which is given by

$$\frac{d\psi_i}{dt} = \frac{1}{R\Sigma}\frac{d}{dR}\left[RD_{\psi_i}\Sigma\frac{d\psi_i}{dR}\right] \tag{5}$$

where $\psi_i (= \epsilon_i)$ is the dust-to-gas ratio for the $i$'th dust species, $D_{\psi_i} = \nu / Sc_{\psi_i}$ ($Sc$ is the schmidt number). For gas tracers $Sc_\psi = 1$, and for dust

$$Sc_{\psi_i} = \frac{(1 + St_i^2)^2}{1 + 4St_i^2} \tag{6}$$

So far this has not included radiation pressure and simply assumed the natural orbital velocity of the dust to be keplerian. For this project I therefore adapt the equations and the model to include the radiation pressure.

## 2.1 Radiation Pressure

We characterise the radiation pressure with a parameter $\beta = \frac{|F_{rad}|}{|F_{grav}|}$ this can indicate how sub-keplerian the dust is. A similar parameter $\eta$ exists for the gas pressure, resulting in the azimuthal velocities $v_{d,\phi}$ for the dust and $v_{g,\phi}$ for the gas being [Marino et al., 2020]:

$$v_{d,\phi} = v_k(1 - \beta)^{1/2} \tag{7}$$

$$v_{g,\phi} = v_k(1 - \eta)^{1/2} \tag{8}$$

Where $v_k$ is the Keplerian orbital velocity and

$$\eta = -\frac{1}{R\Omega_k^2 \rho_g}\frac{dP_g}{dR} \tag{9}$$

Where $\Omega_k$ is the Keplerian angular velocity, $\rho_g$ and $P_g$ the gas density and pressure. We can see that whether the dust orbits slower or faster than the gas relies on whether $\beta > \eta$ or $\beta < \eta$, this then determines whether the dust moves inwards or outwards, as described in section 1.3

$\beta$ can be expressed as $\beta = \frac{CL_\star}{\rho_s D M_\star}$ ($\rho$ and $D$ the density and diameter of the dust grains, $C$ a constant), the important relation here being $\beta \propto 1/D$

We can take Equation 7 to first order in the radiation pressure parameter $\beta$ to get the dust azimuthal velocity due to the radiation pressure

$$v_{dust,\phi} = v_k\left(1 - \frac{1}{2}\beta\right) \tag{10}$$

This $-\frac{1}{2}\beta v_k$ term is the one that we include in the equations of motion in order to get the radiation pressure effect.

To add in the effect of radiation pressure on the dust-gas dynamics we follow the derivation from [Dipierro et al., 2018] and add in the radiation pressure terms. The dust and gas velocities are expressed as perturbations around the local Keplerian velocity $v_k = r\Omega_k \mathbf{e}_\phi$. The equations of motion, when assumed in steady state, can be written as:

$$u_\phi = -\sum_i \frac{\rho_{d,i}}{2\rho_g St_i}(v_{r,i} - u_r) + \frac{1}{2}v_p \tag{11}$$

$$u_r = \sum_i \frac{2\rho_{d,i}}{\rho_g St_i}(v_{\phi,i} - u_\phi) + v_{visc} \tag{12}$$

$$v_{\phi,i} = \frac{v_{r,i} - u_r}{2St_i} - \frac{1}{2}\beta_i v_k \tag{13}$$

$$v_{r,i} = -\frac{2(v_{\phi,i} - u_\phi)}{St_i} \tag{14}$$

Where the $i$'s represent the different dust species, $u_\phi$ is the gas azimuthal velocity, $u_r$ is the gas radial velocity, similarly for $v_{\phi,i}$ and $v_{r,i}$ for the $i$'th dust species, velocities being relative to the keplerian velocity. The $\rho$'s are the densities, and $St_i$ is the stokes number (dimensionless stopping time) of the $i$'th dust species. In addition

$$v_p = \frac{1}{\rho_g \Omega_k}\frac{\partial P}{\partial r} \tag{15}$$

$$v_{visc} = \frac{2}{\rho_g \Omega_k}\nabla \cdot \sigma \mid_\phi \tag{16}$$

The $\frac{1}{2}\beta_i v_k$ is the added radiation pressure term, derived above, with $\beta_i$ being the radiation pressure parameter for the $i$'th dust species.

Equations 11-14 can be solved simultaneously to give the following gas velocities:

$$u_\phi = \frac{1}{2}\left[\frac{(1+\lambda_0)v_p + \lambda_1 v_{visc} - [\mu_0(1+\lambda_0) + \mu_1\lambda_1]v_k}{\lambda_1^2 + (1+\lambda_0)^2}\right] \tag{17}$$

$$u_r = \frac{-\lambda_1 v_p + (1+\lambda_0)v_{visc} + [\mu_0\lambda_1 - \mu_1(1+\lambda_0)]v_k}{\lambda_1^2 + (1+\lambda_0)^2} \tag{18}$$

and the following velocities for the $i$'th dust species:

$$v_{\phi,i} = \frac{u_\phi - \frac{1}{2}u_r St_i - \frac{1}{2}\beta_i v_k St_i^2}{St_i^2 + 1} \tag{19}$$

$$v_{r,i} = \frac{u_r + 2u_\phi St_i + \beta_i v_k St_i}{St_i^2 + 1} \tag{20}$$

The contributions to the gas velocities from the individual dust species is via the $\lambda_j$ and $\mu_j$ parameters defined as

$$\lambda_j = \sum_i \epsilon_i \frac{St_i^j}{St_i^2 + 1} \tag{21}$$

$$\mu_j = \sum_i \epsilon_i \beta_i \frac{St_i^j}{St_i^2 + 1} \tag{22}$$

$\epsilon_i$ being the dust-gas ratio of the $i$'th dust species

We can then express the difference in radial velocity between a given dust species and the gas

$$\Delta v_{r,i} \equiv v_{r,i} - u_r = \frac{2u_\phi - u_r St_i + \beta_i v_k}{St_i + St_i^{-1}} \tag{23}$$

These expressions are then what is implemented in the code.

## 2.2 Dust and Gas Input

For this project I added a module to deal with inputting dust and gas into the simulation, which is thought to come from collisions in a planetesimal belt.

I included 3 different modes of input:

- In a single cell
- Uniformly by mass over a range of cells
- Following a gaussian profile with a given FWHM

The "width" of the input will henceforth mean the width in AU of the input region for the second case, and the FWHM for the third case. This width can be varied. These different modes are used in various simulations, and we will discuss the effects of each one.

Of these 3 input methods the last is of course the most realistic, however it is also more costly in

terms of run-time for the simulation, so when the first two methods will do, it can be worth using those instead.

Other capabilities I gave this module are to chose the radius at which the dust and gas are inputted (these can be different) and to be able to chose a range of dust sizes. When including multiple dust sizes, mass is added evenly between the different species, this follows a number density power law $n(D) \propto D^{-3}$ (with $D$ the dust grain diameter).

## 2.3 Testing the model

We test the additions to the code in two simple situations (with and without radiation pressure) not including the feedback of the dust on the gas. To test these we first need to derive some analytical relations between the dust and gas densities.

We use the formula for steady state surface density [Pringle, 1981] here applied to the dust being modeled as a fluid

$$\dot{M} = 2\pi\Sigma_d R v_r \tag{24}$$

where $v_r$ is the absolute value of the radial velocity. In a steady state $\dot{M}$ will be a constant through the disc, so in terms of radial dependence

$$\Sigma_d \propto \frac{1}{R v_r} \tag{25}$$

Now from [Weidenschilling, 1977] we have that the radial velocity is different depending on what regime the Stokes number is, this can be seen in the expression [Birnstiel et al., 2012]

$$v_r = \frac{v_p}{St + St^{-1}} \tag{26}$$

With $v_p$ as defined in Equation 15.
We see that for $St << 1$, $v_r = v_p St$. Here the limiting factor is the radial terminal velocity attained by dust grains, and for $St >> 1$, $v_r = v_p/St$. Here the limiting factor is the strength of the azimuthal coupling between the dust and gas.
We now investigate how these vary with radius $R$, and assume that quantities scale as power laws. From Equation 15 we can therefore get

$$v_p \propto \frac{P(R)}{R\rho_g(R)\Omega_k(R)} \tag{27}$$

We take a blackbody temperature for the gas, so $T \propto R^{-1/2}$ [Marino et al., 2020]. We also use the following relations: $P/\rho_g = c_s^2$ ; $c_s = \sqrt{\frac{\mathrm{R}T}{\mu}}$ (here R is the gas constant, not radius) and $\Omega_k \propto R^{-3/2}$ Combining these we get that $v_p$ is constant withe respect to $R$

Now the Stokes number can be expressed as [Birnstiel et al., 2012]

$$St = \frac{\pi a \rho_s}{2\Sigma_g} \tag{28}$$

where $a$ is the dust diameter and $\rho_s$ is the dust's internal density, so both are independent of $R$. Hence $St \propto \Sigma_g^{-1}$. So we can now express the relation between our dust density and the gas density

when in steady state: For $St << 1$ $\Sigma_d \propto \frac{\Sigma_g}{R}$ and for $St >> 1$ $\Sigma_d \propto \frac{1}{R\Sigma_g}$

When including radiation pressure, equation 26 will be altered as in equation 20 to include a $\beta v_k$ on the numerator, this will add an extra $R^{1/2}$ dependence meaning that for $St >> 1$ we will have $\Sigma_D \propto \frac{1}{R^{1/2}\Sigma_G}$.

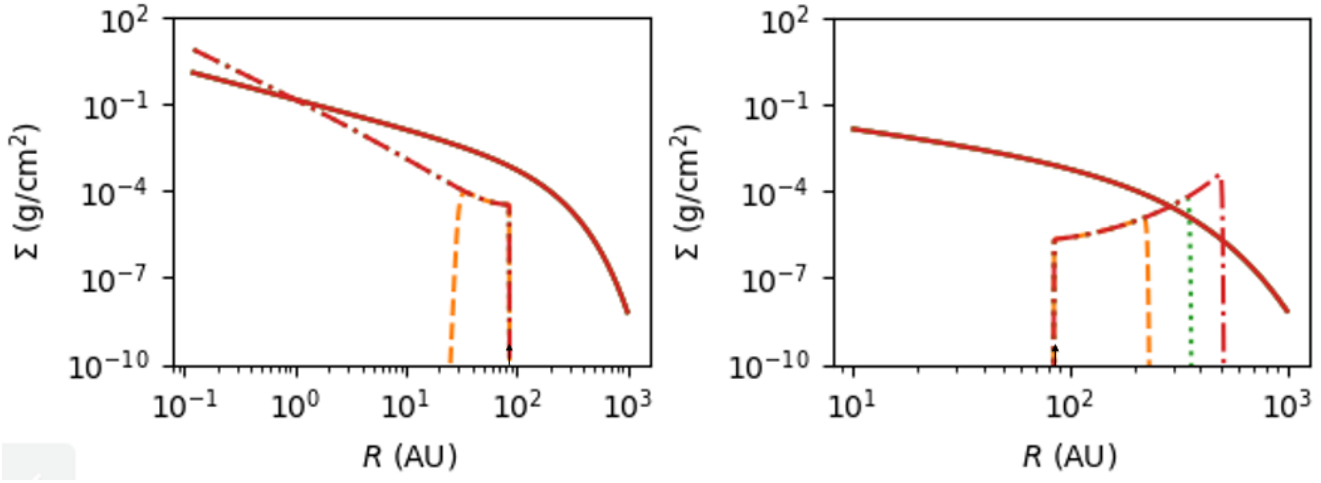


Figure 2: Solid line is gas surface density, dashed lines are dust, yellow (dashed) = $10^4$yrs, green (dotted) = $10^5$yrs red (dash-dotted) = $10^6$yrs. Left: No radiation pressure and no feedback, $St < 1$. Right: Radiation pressure included but no feedback, $St > 1$. Black arrow at the input location.

To test the additions to the model, we run some simulations without the dust feedback, this way we can verify the simulations against the analytical results just derived. These are shown in Figure 2. In the left hand simulation we calculated the gradients at 17au: $\Sigma_d \propto R^{-2.18}$ and $\Sigma_g \propto R^{-1.17}$ (this agrees with $\Sigma_d \propto \frac{\Sigma_g}{R}$). In the right hand simulation we calculated the gradients at 151au: $\Sigma_d \propto R^{2.03}$ and $\Sigma_g \propto R^{-2.52}$ (this agrees with $\Sigma_d \propto \frac{1}{R^{1/2}\Sigma_g}$). Both of these results are therefore in agreement with the analytic calculations given the local $\Sigma_g$ scalings. The graphs are in opposite Stokes regimes so that we can see the result more clearly.

As we present results, many graphs will be shown. Most will be of the same type as the ones above meaning that we look at the gas and dust surface densities, the gas being shown in solid lines, and the dust in dashed/dotted lines.

# 3 Results

We will now begin to present various results from simulations and give some interpretations. In these simulations the stellar properties remain the same, we use a radius $R_\star = 2.5R_\odot$, an effective temperature $T_\star = 6500$K, and a mass $M_\star = 2M_\odot$.

The main parameters that we vary are: the dust and gas input rates, the type/width of input, and the viscosity.

There are also some parameters that will often take the same value but are occasionally changed to emphasise a certain feature, or to maintain us in the physical regime we are investigating. These are the total initial gas mass (usually $10^{-5}M_{\odot}$), the dust and gas input radius (usually 85au), and the diameter of the dust grains (usually $10\mu$m).

One key finding we will present is the following evolutionary pathway:

- Dust (of appropriate size) input into a gas disc will drift outwards and form a ring.
- The formation of the ring is coincident with (and due to) gas being pushed inwards.
- This gas will accumulate at the dust input location, potentially trapping dust there.
- Depending on the strength of the dust trapping, the dust ring may grow inwards, or drift outwards.

Other findings are:

- Viscosity will affect this pathway, in particular the gas buildup and the dust trapping.
- A high gas input will prevent the dust from forming the ring, instead the dust moves outwards with the edge of the disc formed by the input gas.
- Multiple dust species can give rise to more complex structure such as multiple rings

One phenomenon that will arise many times is the effect of a steep drop in gas density. Gas pressure will have some (positive) power-law dependency on density through an equation of state, the result being that a gas density gradient is equivalent to a gas pressure gradient. From equation 9 we have

$$\eta \propto -\frac{dP_g}{dR}$$

Therefore, in a steep negative pressure gradient, the gas will have a very high $\eta$ value. The mechanism through which our dust drifts out (as described in sections 1.3 and 2.1) relies on $\beta > \eta$, so dust will not be able to cross a very steep gas density gradient. A reasonably steep gas gradient will slow the dust drift velocity and equivalently decrease the amount of dust that can cross it.

## 3.1 Introducing dust into low viscosity discs

For now we restrict the problem to a single dust size of 0.001cm ($10\mu$m). We start by investigating low viscosity discs, in the [Shakura and Sunyaev, 1973] $\alpha$ prescription we take $\alpha = 10^{-8}$, this is small enough that viscous effects will not be seen.

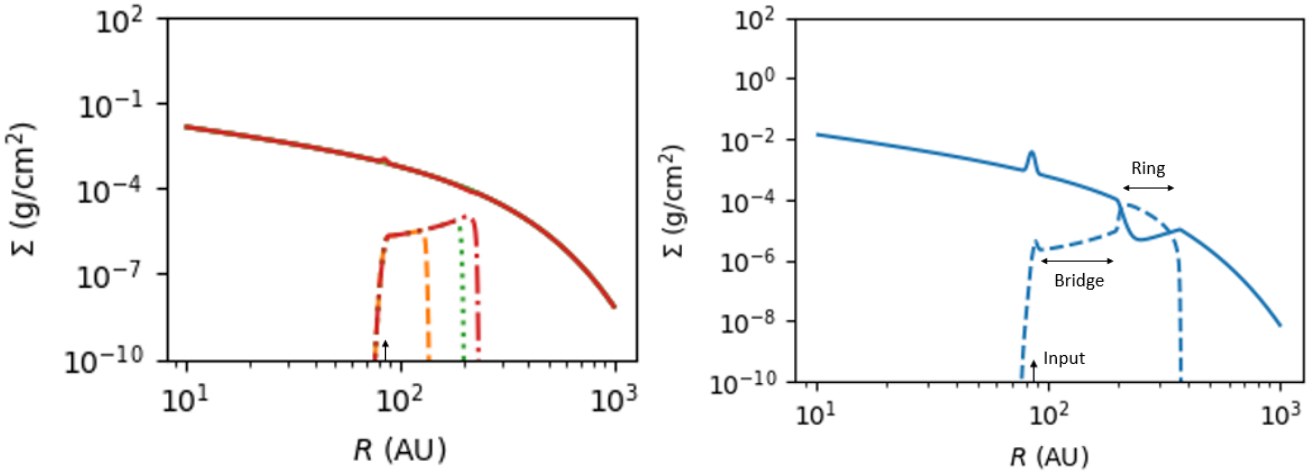


Figure 3: Solid line is gas surface density, dashed lines are dust. Left: yellow (dashed) = $10^3$yrs green (dotted) = $5 \times 10^3$yrs, red (dash-dotted) = $10^4$yrs. Right: blue = $10^5$yrs. Black arrow at the input location. Right hand plot shows the areas we refer to as the "Input region", the "Bridge" and the "Ring".

The first results showing the dust and gas evolution are shown in Figure 3. Once the dust is input, it is pushed out due to the mechanism described in section 1.3. Initially, while the dust surface density is much lower than the gas surface density (ie: the dust-to-gas ratio $\epsilon$ is very low) the loss of angular momentum is barely felt by the gas, so there is only a minimal feedback effect on the gas. So at early times the dust is simply flowing outwards, following the profile that would be expected in the no-feedback limit and there is very little effect on the gas. This can be seen in the left hand plot of Figure 3, which is quite similar to the right hand plot of Figure 2.

The dust density increases with radius, so eventually a point is reached where the dust-to-gas ratio approaches unity. Feedback then starts to have a significant effect on the gas. The gas begins to lose a significant amount of angular momentum and so is pushed inwards, and consequently the gas density decreases at this point. The gas cannot move further in than the dust input radius, as in the absence of viscosity the only mechanism for the gas to move inwards is being torqued down by dust, so we get a build-up of gas at the input radius. This is seen in the right hand plot of Figure 3.

Since the gas density drops when there starts to be a significant dust-to-gas ratio, this ratio reaches and then exceeds 1 as the gas density keeps dropping. The very high dust-to-gas ratio achieved has the reverse effect from before, in this region the gas now loses significant angular momentum, but the dust does not gain very much, so it has a low outwards radial velocity. Surface density is inversely proportional to radial velocity in a steady state (from equation 25). Although we are not quite in steady state here, the rough inverse relation of $\Sigma$ and $v_r$ still holds, we can think of an analogy: a large group of joggers (evenly spaced out) come across some mud which slows them down, the density of joggers will therefore be higher in the mud, and the density gradient will be sharp if the mud starts suddenly. So the dust builds up here and we have a ring of dust, the density gradient between this ring and the bridge of dust feeding it is quite steep, so the ring is well defined. The dust in the ring, follows the profile of the gas that had been there initially, this is because of the conservation of angular momentum. Since the dust is given its angular momentum by the gas, it cannot end up with more than the gas initially had, so the dust density will be capped and will move out along the original gas profile.

This is a key result: a dust ring forms some distance out from the dust input. This happens very reliably, regardless of parameter choice. This dust ring is accompanied by a gap/well in the gas density, we note that through the ring the gas density is low but is increasing with radius. We will investigate the subsequent evolution of this dust ring, but to do this we first notice that in the right hand plot of Figure 3, there is a slight spike in the dust density at the input radius. This is due to the dust trapping effect of the gas building up at the input radius.

We have seen that the gas starts building up at the input radius as it can't get pushed further in. This causes steep gas density gradients on either side of this build-up, and we have already noted that a steep gas gradient prevents, or at least lowers the outwards flux of dust

The gas building up at the input radius causes the radial velocity of the dust being pushed out to decrease. This dust trapping has the effect of both increasing the dust density at the input radius and reducing the amount of dust that drifts outwards, in turn affecting the dust morphology at larger radii.

We have so far identified 3 main features of the dust distributions and we will often refer to these in the following terms (as illustrated in the right hand plot of Figure 3). We have the "ring" that forms at a large radius; the "dust trap", "dust spike" or simply "dust input/input region" where the dust is input and will sometimes get trapped, forming a spike, and we have the "bridge" which links the two. There are a few occasions where the dust trapping effect is not at the input location, at which point "dust trap/spike" and "dust input" are no longer the same. It will be clear to which we are referring.

If we have very strict dust trapping then very little mass will be escaping the input region, this means that there will be very little mass that can move through the bridge and into the ring. In this case the ring will effectively stop growing inwards once the dust-trapping effect has taken hold. In general the ring will always keep growing/spreading outwards. If instead the dust trapping is less strict and there is a significant mass flux out of the input region, then the ring will keep growing inwards in the following way. The inner edge of the ring has a steep gas gradient, so as the dust arrives there it slows down and so its density increases, which then means the dust ring grows inwards, this then pushes the gas that is at that location inwards, meaning that the gas gradient also moves inwards to allow this effect to continue.

A good illustration of this is Figure 4. Here we compare two different scenarios, the left plot having a wide smooth input, and the right plot having a narrow sharp input. We know that this will mean that the latter will have a much stronger dust trapping effect since we will get a steeper gas gradient at the edge of the input region. From equation 24, we see that the mass flux has the form

$$\dot{M}_d \propto \Sigma_d v_r R$$

We use this to compare the relative mass fluxes in the different parts of the disc.

The differences between the two sides of Figure 4 are quite clear. The lesser dust trapping disc (LHS) has a higher $v_{r,d}$ in the dust trap than in the ring (middle left), so dust escapes the input more effectively than it travels through the ring. The mass flux in the bridge is therefore higher

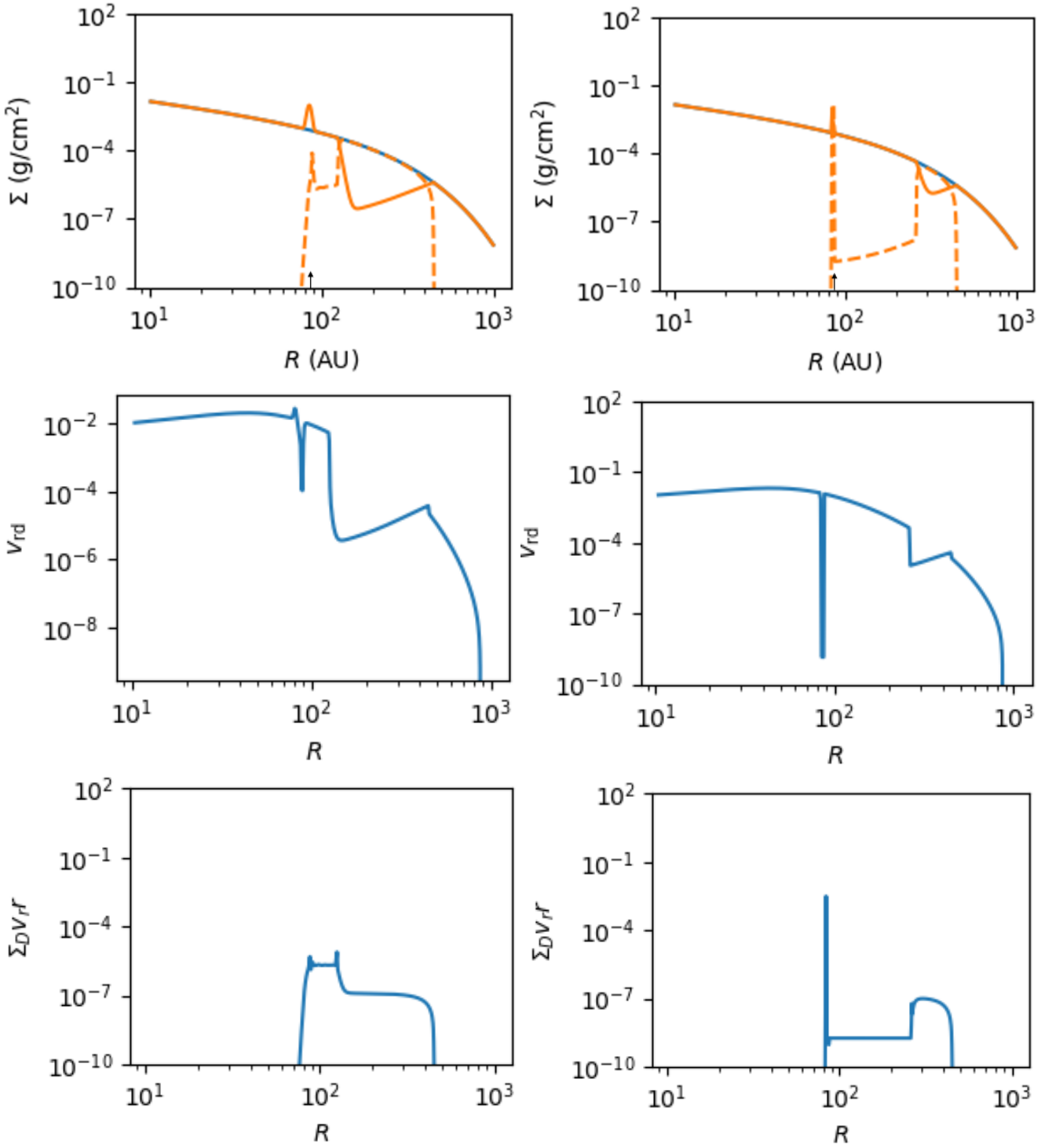


Figure 4: Time $= 3\times10^5$yr. Comparison of the surface densities (top row) the dust radial velocities (middle row) and the local dust mass flux (bottom row) for two different set-ups. Left: Gaussian dust input with a width of 5au (wide and smooth), so dust is not trapped at the input radius instead it will move outwards and accumulate at the inner edge of the ring. Right: Uniform input of width 1.5 au (narrow and sharp), so dust trapping is important and the ring stops being fed. Black arrow at the input location.

than the mass flux in the ring (bottom left). The bridge therefore will have a reasonably high density and the ring grows inwards as the dust from the bridge builds up at the inner edge of the ring (top left). In contrast, the higher dust trapping disc (RHS) has a lower $v_{r,d}$ in the spike than the ring (middle right), so dust escapes the input less effectively than it moves through the ring. The mass flux in the bridge is then lower than in the ring (bottom right) so less mass arrives at the inner edge of the ring than leaves, so the ring moves outwards (top left).

We have therefore shown that it is the strength of the dust trap, and hence the nature of the input, that determines which way the dust ring evolves. The dust trapping does not start straight away so initially all rings will grow inwards, then either keep growing inwards, halt the inwards growth, or revert and be pushed back out.

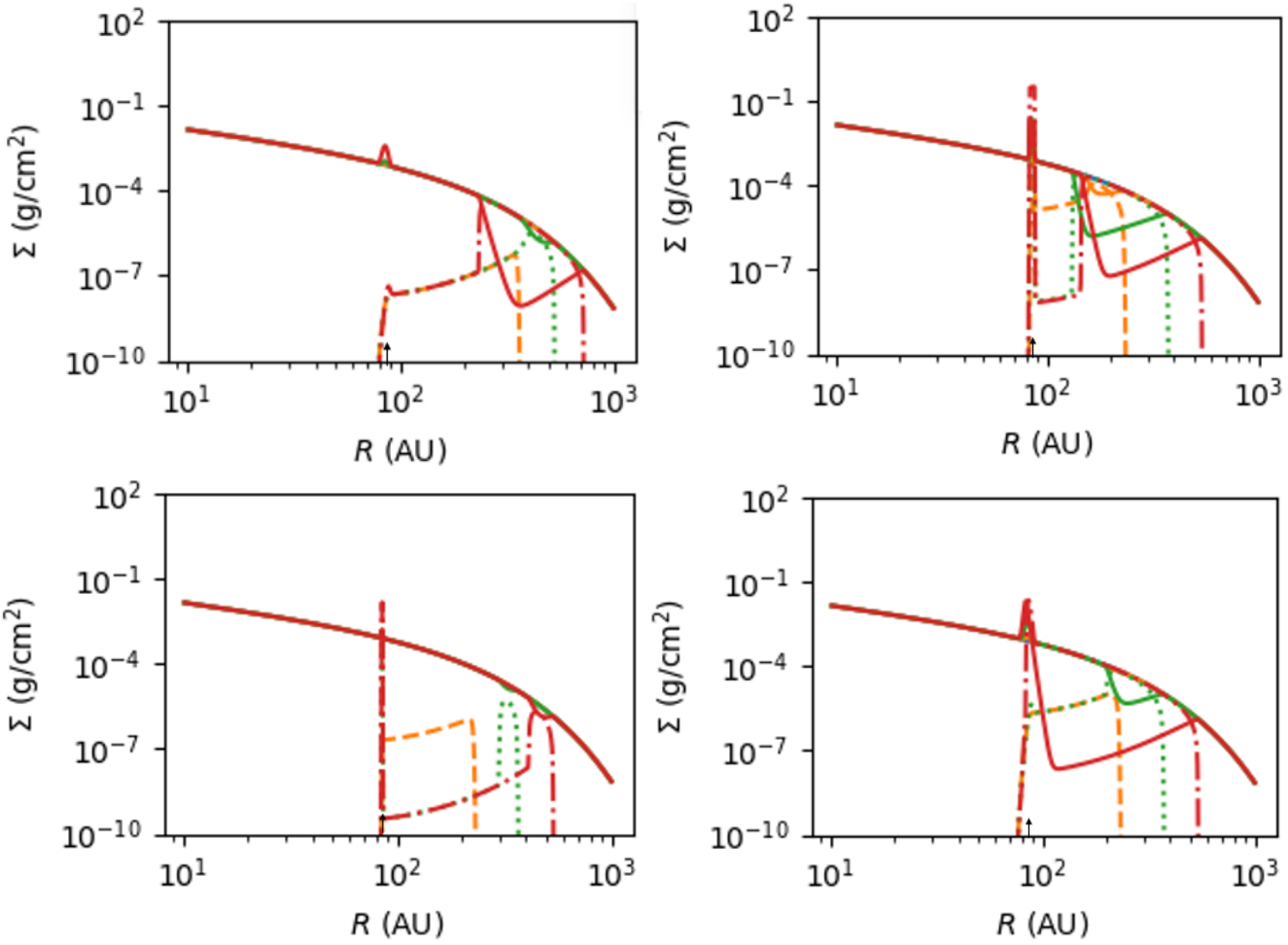


Figure 5: Solid line is gas surface density, dashed lines are dust. Top left: yellow (dashed) = $10^5$yrs, green (dotted) = $10^6$yrs red (dash-dotted) = $10^7$yrs, Gaussian input of width 5au at a rate of $10^{-13}$M$_\odot$/yr For the other 3 graphs: yellow (dashed) = $10^5$yrs green (dotted) = $5 \times 10^5$yrs, red (dash-dotted) = $10^6$yrs. Top right: Uniform input over 2.5 au at a rate of $10^{-10}$M$_\odot$/yr Bottom left: Gaussian input of width 0.5au at rate of $10^{-12}$M$_\odot$/yr Bottom right: Gaussian input of width 5au at rate of $10^{-11}$M$_\odot$/yr. Black arrow at the input location.

In Figure 5 we see the results of 4 simulations in different parts of the parameter space. Each gives a seemingly different outcome, however they all have the common point of initially forming a dust ring. These rings evolve in different ways. The top right plot has a uniform input, so will have a reasonably strong dust trap causing the ring to stop growing inwards, we notice that the inner edge of the ring does not migrate out very much, this will be due to the mass fluxes in the bridge and ring being quite similar. The bottom right plot has a smooth Gaussian input so the gas gradient formed is not so steep and the dust trapping not so strong. The top left plot has a low dust input rate so even after $10^7$ years there has not been a significant enough inflow of gas to cause much of a dust trap so it is still in the initial growth stage. The bottom left plot has a very narrow and sharp input, so the dust trapping effect is strong, this combined with a low dust input rate means only a narrow ring is formed, this then does not grow inwards, but instead migrates outwards due to the gas drag effect. We see the ring spreads out a little as it migrates out, this can be thought of as conservation of mass in the ring since the density in the peak decreases, or simply as diffusion.

We again have seen that the dust trapping is exacerbated by the input being narrow, and having sharp edges. Both of these result in the dust input having quite a steep gradient, which means that the profile developed by the gas that has been pushed in will also have a steep gradient, which we have identified as the cause for the dust trapping.

The dust trapping can also be exacerbated by the introduction of a gas input coincident with the dust input. The planetesimals that would be responsible for the dust input can often have gas trapped in ice that can be released as discussed in the introduction. Inputting this gas at the input radius will cause the steep gas gradient responsible for dust trapping to form earlier and be more pronounced, leading to a stronger and earlier dust trap. The first few plots of Figure 7 illustrate a strong and early dust trap.

## 3.2 Introducing viscosity and a localised gas input

So far we have only considered the dynamics of low viscosity discs with only a dust input. In this section we investigate what changes increasing the viscosity makes to our current model of a disc's evolution. We will compare different viscosities by having $\alpha$ range from $10^{-8}$ to $10^{-1}$. We will also investigate different gas input rates relative to the dust input rate, using a Gaussian input of 5au. A low gas input rate will mean that by the end of the simulation, most of the gas present was already there when the dust started being added (ie Primordial gas), whereas with a high gas input, most of the gas present by the end of the simulation has been added alongside the dust (ie Secondary gas).

We first consider a case where the same mass of gas is input as of dust, with a significant total initial gas mass. This is shown in Figure 6. The input gas density being low in comparison with the total already there means that the input gas will have minimal effect. This means that this simulates a hybrid disc with mostly primordial gas content.

We then vary the viscosity, at early times there is little effect. The yellow profile is the same throughout. At intermediate times, the formation of the dust ring still occurs up to a viscosity of $\alpha = 0.01$, although with a higher viscosity the ring is less clearly defined, in particular with a less severe inner boundary, this can be seen in the green profiles. At late times there is a significant change. For low viscosities, the gas is pushed in by the outflowing dust (as in section 2.1), as

viscosity is increased this is counteracted by the viscous spreading, so the steep gas gradient is not pushed all the way in to the input region. There is no dust trapping at the input, so the dust keeps feeding the ring. At high viscosities the gap/well in the gas densities gets filled in (partially for $\alpha = 10^{-2}$ and completely for $\alpha = 10^{-1}$) resulting in the dust ring being less pronounced as the higher gas density can keep pushing the dust out more effectively.

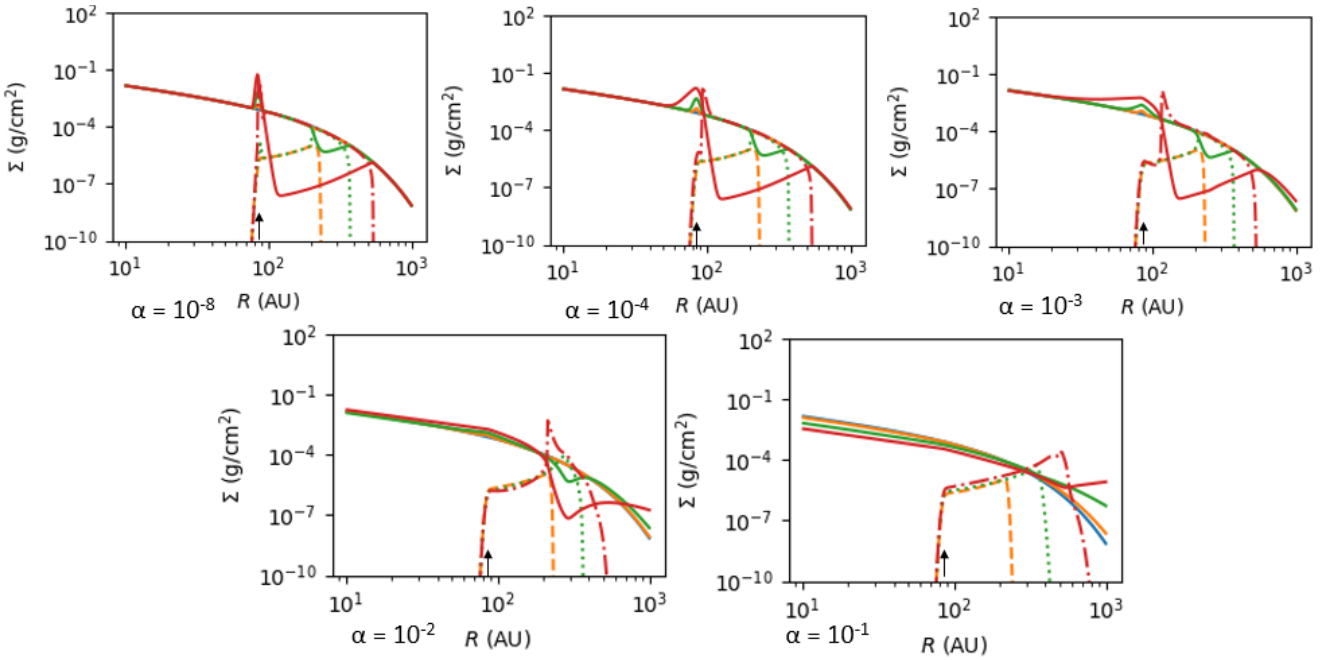


Figure 6: Total gas mass of $10^{-5}M_{\odot}$, dust and gas both input at a rate of $10^{-11}M_{\odot}$/yr, yellow (dashed) = $10^4$yrs, green (dotted) = $10^5$yrs, red (dash-dotted) = $10^6$yrs, $\alpha$-viscosity variation on plots. The ratio of initial mass to total added mass is 1. Black arrow at the input location.

One aim of this project is to assess whether the dynamical effect of dust pushing gas inwards could replicate viscous effects, meaning that previous estimates of viscosity in such discs might have been over-estimates. Our results show that at low viscosity there is no effect on gas inside the input region, so it is unlikely that estimates of viscosity in the inner regions of discs such as $\beta$-Pic are affected by this mechanism.

With a high viscosity of $\alpha = 0.1$ as is the lower bound estimate for $\beta$-Pic [Kral et al., 2016], the dust ring cannot form because the viscosity quickly damps out a dip in gas density which is what allows the dust ring to form. We see that the dust profile keeps rising, roughly following the path of the case with no feedback between the dust and the gas. This is interesting as it means this dust-ring forming mechanism is unlikely to be at play in the formation of structure in high-viscosity discs such as $\beta$-Pic

To simulate a hybrid disc with mostly secondary gas content, we include little initial gas and use a high gas input. The results are shown in Figure 7. As expected, the high gas input causes dust trapping to occur very early, so in the first two (low viscosity) plots most of the dust is trapped in the input region, with only a very small amount having escaped.

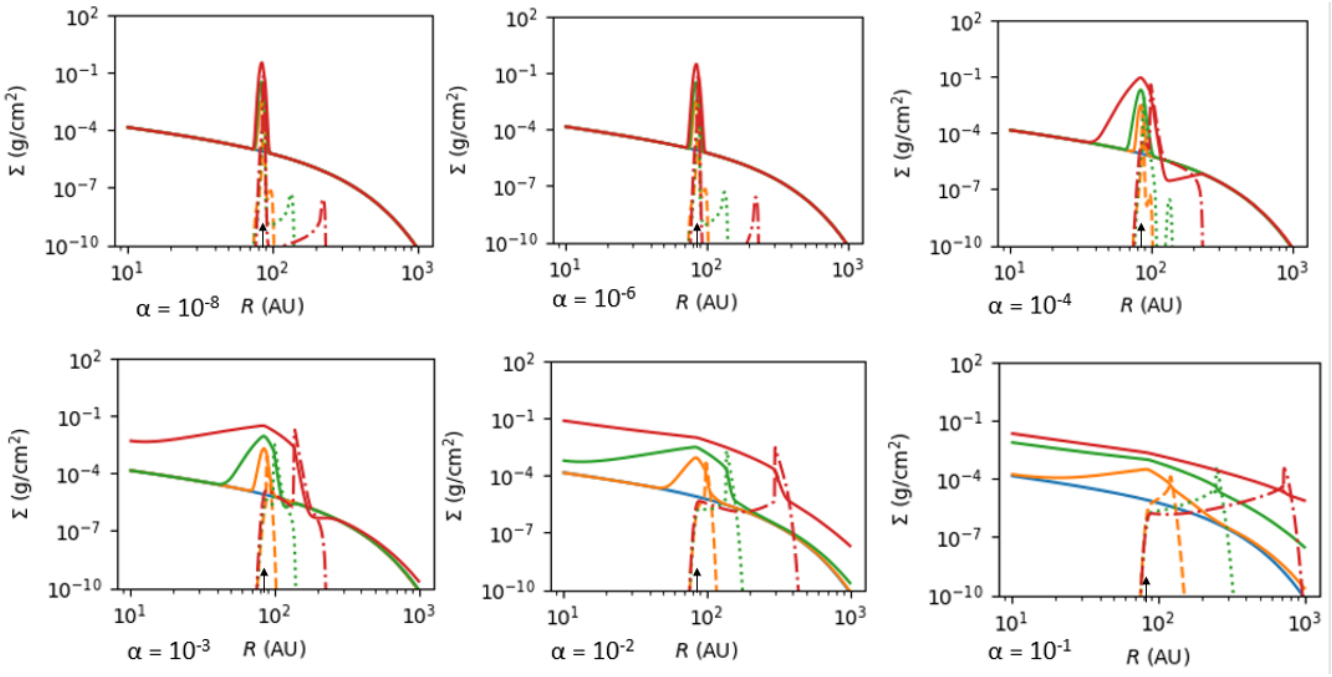


Figure 7: Total gas mass of $10^{-7}M_{\odot}$, dust input at a rate of $10^{-11}M_{\odot}$/yr, gas input at a rate of $10^{-10}M_{\odot}$/yr, yellow (dashed) = $10^4$yrs, green (dotted) = $10^5$yrs, red (dash-dotted) = $10^6$yrs, $\alpha$-variation on plots. The ratio of initial mass to total added mass is $10^{-3}$. Black arrow at the input location.

At higher viscosities, the gas spreads out, and since there is very little initial gas, a disc starts forming from this secondary gas. The dust-gas drag slows the migration of the outer edge of this disc, and the dust accumulates at this outer edge. It cannot migrate any further as there is a steep gas gradient here which, as in the dust trap, means that $\eta \sim \beta$. This is an example of the effect described by [Takeuchi and Artymowicz, 2001].

The results from this section are quite promising. For dust released into a pre-existing gas disc, a dust ring is formed and has an associated gas deficit throughout the ring, a feature of this being the gas density increasing throughout the ring. This is true for all viscosities studied apart from the highest ($\alpha = 0.1$) where the viscosity fills in the gas density deficit. On the other hand, when most of the gas is released alongside the dust, the dust is either trapped at the input (for low viscosities) or forms a narrow ring colocated with a steep gas gradient at the outer edge of the disc. This is promising, as we have discovered a feature, which can help distinguish between the two kinds of discs. Finding these features may be difficult, cold gas far from a star is difficult to detect, and most primordial gas is likely to be $H_2$ which is not detectable. However, with the improvement of telescope facilities such as ALMA and future telescopes that are in development, we are at a stage where some such features might be able to be detected with better precision [Hughes et al., 2018]. Although $H_2$ is not directly detectable, it can collisionally excite CO, so observations of different lines of CO might be able to indicate if $H_2$ is present. Neutral Carbon is also a tracer which can be observed by ALMA so can be another place to look for these observations.

### 3.3 Multiple grain sizes

Realistically, we would probably not expect to get a perfect dust input, with all particles exactly the same size. Furthermore some of the structure seen is quite complex, such as the multiple rings in Figure 1. The natural next step is to look at multiple different grain sizes.

Performing a rigorous investigation of the effect of multiple grain sizes is beyond the scope of this project, so we will present a few results which suggest that a more thorough inquiry is warranted. We have restricted ourselves to the low viscosity case.

The radiation parameter $\beta \propto 1/D$ (D the dust diameter) so the radiation pressure is higher on smaller dust. The Stokes number $St \propto D$ so smaller dust has a lower Stokes number, in the $St >> 1$ regime $v_{r,d} \propto St^{-1}$ (from Equation 26). Both of these reasons mean that the outward radial velocity of small grains should be higher. So we would expect the smaller dust to get further out in a shorter time. Structure formed by small dust is therefore expected to be found at a larger radius than structure formed by large dust. Figure 8 illustrates this idea.

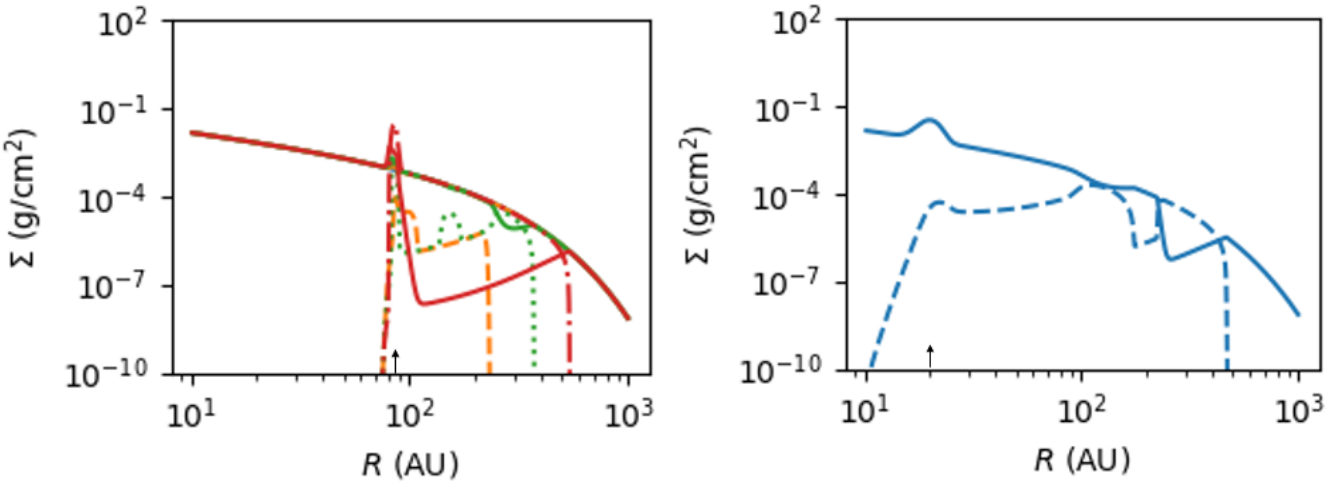


Figure 8: Solid lines are gas density, dashed lines are dust density. Left: dust diameters 10 $\mu$m ($\beta = 0.215$) and 50 $\mu$m ($\beta = 0.043$), yellow (dashed) = $10^4$yrs, green (dotted) = $10^5$yrs, red (dash-dotted) = $10^6$yrs. Right: Dust diameters 5 $\mu$m ($\beta = 0.43$) and 50 $\mu$m ($\beta = 0.043$), time = $10^5$yrs. There is an equal mass of dust of each size. Black arrow at the input location.

We see in the right hand plot of Figure 8 that we have formed two distinct dust rings, a similar 2-humped, camel-like, behaviour is also seen in the green line of the left hand plot. In both these cases, as expected, the outer ring is made up of the smaller dust, and the inner ring of the larger dust.

In left hand plot of Figure 8 the red line looks very similar to the single dust species case once the ring has grown and joined up with the input region (bottom right of Figure 5). We can split the dust density into that of each dust species, this is shown in Figure 9. Here we see that initially each species moves outwards, the smaller one faster, and each form their own ring. By the late stage, the small dust ring has grown inwards and the large-dust ring has seemingly been pushed

inwards. Though initially surprising, this is in fact what has happened.

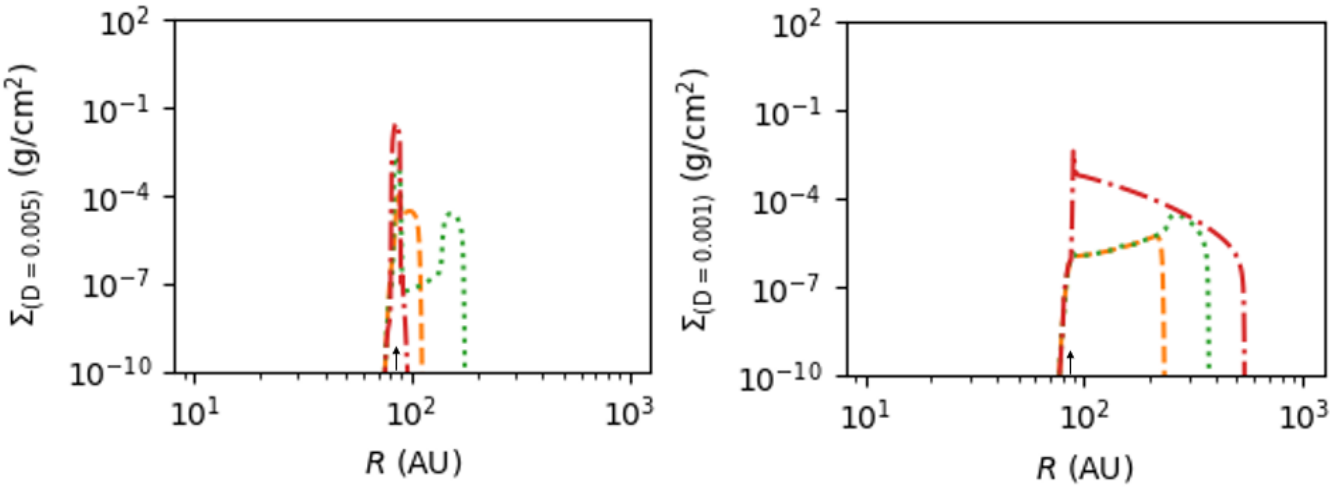


Figure 9: These are the individual dust densities corresponding to the Left hand plot of Figure 8, yellow (dashed) = $10^4$yrs, green (dotted) = $10^5$yrs, red (dash-dotted) = $10^6$yrs. Left: Surface density for the dust of diameter 0.005 cm. Right: Surface density for the dust of diameter 0.001 cm. Black arrow at the input location.

We have already encountered the effect responsible, it is the common culprit, a gas density gradient. In the non-viscous case, we know that when the dust ring forms the gas present is pushed inwards and we get a steep gas gradient at the inner edge of the dust ring. This acts as a barrier to dust. As the outer ring grows and so this barrier is pushed inwards, it sweeps up the inner ring, as the dust in this ring cannot pass through the barrier, meaning the inner ring is pushed all the way back to the input region. This is similar to the effect described by [Takeuchi and Artymowicz, 2001] which we have mentioned before, but whereas in the previous section, the gas disc was spreading, and the dust with it, here the gas disc is contracting and the dust being dragged along with it.

We have seen that multiple dust species being released could account for more complicated structure in hybrid discs, such as multiple rings.

# 4 Caveats

Before concluding, let us consider some of the assumptions and simplifications we have made in this project, and the limitations they may cause.

One clear major simplification is the use of invariant dust grain sizes, whether there is one size or multiple sizes. In reality dust grains will collide, leading to either grain growth or fragmentation, depending on the type of collisions. In debris discs it is expected that collisions would mostly fragment grains rather than cause sticking, but we shall still consider both.

To assess how this simplification has affected our results we can estimate the timescales on which each of these two effects act.

## 4.1 Grain growth

Grain growth is dependent on the collisions resulting in sticking, which is not certain, particularly in debris discs. However we will still look at its timescale [Birnstiel et al., 2012]

$$t_{grow} \sim (\epsilon \Omega_k)^{-1} \tag{29}$$

Where $\epsilon$ is the dust-gas mass ratio. We can use the keplerian velocity as, although the dust is sub-keplerian, its velocity will still be of the same order of magnitude as $\Omega_k$. In our case:

$$t_{grow} \sim \frac{0.1}{\epsilon} \left( \frac{R}{\text{au}} \right)^{3/2} \tag{30}$$

In the "dust bridge" of our model, connecting the input to the dust ring, $\epsilon \lesssim 10^{-4}$ and so with the input radius at 85au we can write the following for dust there:

$$t_{grow} \gtrsim 10^6 \text{years} \tag{31}$$

This is of a larger order of magnitude it than takes for the dust to form a ring. A lower dust input can get the ring to form slower, however this also lowers $\epsilon$ in the bridge, so it would increase the growth timescale too. So there should not be much of an effect on ring formation.

In the ring itself and in the dust trap, $\epsilon$ will eventually get much larger, in the ring this will in part be counteracted by the larger orbital radius, however grain growth would still likely speed up. This would lead to a lower mass flux across the ring, which would in fact only help the ring grow inwards. In the dust trap this might lead to less dust escaping the input region, however with the constant release of new dust this would need careful consideration.

So if the dust collisions result in grain growth, though this might happen on relevant timescales in the latter stage of evolution, it should not drastically affect our results, other than being one extra factor to consider in whether a ring grows inwards or outwards.

## 4.2 Grain Fragmentation

The collision time in a disc of single-sized particles is [Strubbe and Chiang, 2006]

$$t_{coll} \sim \frac{1}{\Omega \tau} \tag{32}$$

Where $\tau$ is the optical depth (perpendicular to the disc plane).
$\Omega \propto r^{-3/2}$ and standard power laws for optical depth in Debris Discs are $r^{-3/2}$ and $r^{-5/2}$ [Strubbe and Chiang, 2006], so $t_{coll}$ will very quickly increase with radius, so we only really need to consider the input location.

In [Strubbe and Chiang, 2006] they model the release of dust and get a maximum optical depth of $\tau = 3 \times 10^{-3}$, only over a very small region, the majority of the disc having optical depth less

than $\tau = 10^{-4}$

A strong upper bound on the optical depth would be $\tau = 0.01$, any higher than this and we would no longer be in a optically thin regime. This means that at our input we have a strict minimum collision timescale of 8000 years. Though this is quite short it should also not be a great problem. Initially as the dust starts to be released, the optical depth will be much lower (by at least a few orders of magnitude bringing the timescale to at least $10^6$ years) so the initial ring formation will not be affected. Fragmentation will therefore only really be important once the dust trapping starts, at which point what happens to the dust inside the trap is not very relevant.

Fragmentation may also eventually have an effect in the ring. A possible effect of this would be to cap the outer edge of the ring with the dust fragmenting and being blown out preventing the ring from expanding past a certain radius. In a case where the dust trapping stops the ring from growing at the inner edge, fragmentation could perhaps cause the ring to dissipate, this might be interesting to investigate further, finding the lifetime of such rings and hence whether we might expect to observe them.

### 4.3 Other assumptions

We have not included Poynting-Robertson drag here. The P-R drag force is

$$\mathbf{F}_{pr} = \beta F_{grav} \left[ -\frac{2v_r}{c}\mathbf{e}_r - \frac{v_k}{c}\mathbf{e}_\phi \right] \tag{33}$$

where c is the speed of light. Both these terms are very small compared to the values in equations 19/20 for the dust velocities due to radiation pressure and gas drag. Hence, P-R drag can be safely omitted.

The dust released in the planetesimal belt is from collisions, this could lead to a range of eccentricities, however eccentricity is damped on a timescale $t_{damp} \sim P/St$ (P is orbital period), and since here we are in the regime of $St >> 1$ eccentricity is damped faster than the orbital period, so we can safely assume circular orbits. The circularisation may lead to a spread of orbital radii, but since we use a gaussian input for the dust, this is at least partly accounted for.

## 5 Conclusions

We have taken some important steps in the modelling of hybrid discs by including the dynamical back-reaction of the dust on the gas, and have found some evolutionary pathways for them in a variety of configurations. The main result here is finding a new class of gas-dust morphology, where a density maximum in the dust (ie a ring) is accompanied by a density minimum in the gas. This requires the amount of gas added with the dust to be minimal compared to the amount already there.

This ring formation, coupled with the fact that more complicated setups such as multiple grain sizes can give rise to structures such as multi-ringed discs (which are observed and of interest) means that this avenue is worth pursuing further.

This project identified a difference in between dust being released into a pre-existing gas disc,

and dust being released at the same time as a gas disc is forming. In a pre-existing disc, as in Figure 6, we have a dust ring essentially extending from the edge of the gas disc outwards (or in a corresponding gas dip), the hallmark being the anti-correlation of the dust and gas. In a forming disc, the dust ring is coincident with the edge of the gas disc as in 7. This could provide a meaningful way to distinguish between those hybrid discs whose gas is primordial and those whose gas is secondary.

This area of research is a popular one at the moment, further investigation building on this may involve:

- Including dust growth and/or fragmentation.
- Including more dust species or multiple dust release locations corresponding to multiple dust producing belts, this could give more complex structure.
- The effect embedded planets might have on this. Most systems are thought to have planets, the effect of which could alter the mechanism described in this project.
- Better resolution of observations may help identify the edges of the gas discs and where dust rings are in relation to these which as described above could be a promising way of categorising hybrid discs.

# References


[Birnstiel et al., 2012] Birnstiel, T., Klahr, H., and Ercolano, B. (2012). A simple model for the evolution of the dust population in protoplanetary disks. *Astronomy & Astrophysics*, 539:A148.

[Booth et al., 2017] Booth, R. A., Clarke, C. J., Madhusudhan, N., and Ilee, J. D. (2017). Chemical enrichment of giant planets and discs due to pebble drift. *Monthly Notices of the Royal Astronomical Society*, 469(4):3994–4011.

[Dent et al., 2005] Dent, W., Greaves, J., and Coulson, I. (2005). Co emission from discs around isolated haebe and vega-excess stars. *Monthly Notices of the Royal Astronomical Society*, 359(2):663–676.

[Dent et al., 2014] Dent, W. R., Wyatt, M., Roberge, A., Augereau, J.-C., Casassus, S., Corder, S., Greaves, J., de Gregorio-Monsalvo, I., Hales, A., Jackson, A., et al. (2014). Molecular gas clumps from the destruction of icy bodies in the $\beta$ pictoris debris disk. *Science*, 343(6178):1490–1492.

[Di Folco et al., 2020] Di Folco, E., Pericaud, J., Dutrey, A., Augereau, J.-C., Chapillon, E., Guilloteau, S., Piétu, V., and Boccaletti, A. (2020). An alma/noema study of gas dissipation and dust evolution in the 5 myr-old hd 141569a hybrid disc. *Astronomy & Astrophysics*, 635:A94.

[Dipierro et al., 2018] Dipierro, G., Laibe, G., Alexander, R., and Hutchison, M. (2018). Gas and multispecies dust dynamics in viscous protoplanetary discs: the importance of the dust back-reaction. *Monthly Notices of the Royal Astronomical Society*, 479(3):4187–4206.

[Fedele et al., 2010] Fedele, D., Van Den Ancker, M., Henning, T., Jayawardhana, R., and Oliveira, J. (2010). Timescale of mass accretion in pre-main-sequence stars. *Astronomy & Astrophysics*, 510:A72.

[Hughes et al., 2018] Hughes, A. M., Duchêne, G., and Matthews, B. C. (2018). Debris disks: Structure, composition, and variability. *Annual Review of Astronomy and Astrophysics*, 56:541–591.

[Kóspál et al., 2013] Kóspál, Á., Moór, A., Juhász, A., Ábrahám, P., Apai, D., Csengeri, T., Grady, C., Henning, T., Hughes, A., Kiss, C., et al. (2013). Alma observations of the molecular gas in the debris disk of the 30 myr old star hd 21997. *The Astrophysical Journal*, 776(2):77.

[Kral et al., 2019] Kral, Q., Marino, S., Wyatt, M. C., Kama, M., and Matra, L. (2019). Imaging [ci] around hd 131835: reinterpreting young debris discs with protoplanetary disc levels of co gas as shielded secondary discs. *Monthly Notices of the Royal Astronomical Society*, 489(3):3670–3691.

[Kral et al., 2016] Kral, Q., Wyatt, M., Carswell, R., Pringle, J., Matra, L., and Juhasz, A. (2016). A self-consistent model for the evolution of the gas produced in the debris disc of $\beta$ pictoris. *Monthly Notices of the Royal Astronomical Society*, 461(1):845–858.

[Lyra and Kuchner, 2013] Lyra, W. and Kuchner, M. (2013). Formation of sharp eccentric rings in debris disks with gas but without planets. *Nature*, 499(7457):184–187.

[Marino et al., 2020] Marino, S., Flock, M., Henning, T., Kral, Q., Matrà, L., and Wyatt, M. (2020). Population synthesis of exocometary gas around a stars. *Monthly Notices of the Royal Astronomical Society*, 492(3):4409–4429.

[Moór et al., 2011] Moór, A., Ábrahám, P., Juhász, A., Kiss, C., Pascucci, I., Kóspál, Á., Apai, D., Henning, T., Csengeri, T., and Grady, C. (2011). Molecular gas in young debris disks. *The Astrophysical Journal Letters*, 740(1):L7.

[Pringle, 1981] Pringle, J. E. (1981). Accretion discs in astrophysics. *Annual review of astronomy and astrophysics*, 19(1):137–160.

[Roberge et al., 2013] Roberge, A., Kamp, I., Montesinos, B., Dent, W. R., Meeus, G., Donaldson, J. K., Olofsson, J., Moór, A., Augereau, J.-C., Howard, C., et al. (2013). Herschel observations of gas and dust in the unusual 49 ceti debris disk. *The Astrophysical Journal*, 771(1):69.

[Shakura and Sunyaev, 1973] Shakura, N. I. and Sunyaev, R. A. (1973). Black holes in binary systems. observational appearance. *Astronomy and Astrophysics*, 24:337–355.

[Strubbe and Chiang, 2006] Strubbe, L. E. and Chiang, E. I. (2006). Dust dynamics, surface brightness profiles, and thermal spectra of debris disks: the case of au microscopii. *The Astrophysical Journal*, 648(1):652.

[Takeuchi and Artymowicz, 2001] Takeuchi, T. and Artymowicz, P. (2001). Dust migration and morphology in optically thin circumstellar gas disks. *The Astrophysical Journal*, 557(2):990.

[Weidenschilling, 1977] Weidenschilling, S. (1977). Aerodynamics of solid bodies in the solar nebula. *Monthly Notices of the Royal Astronomical Society*, 180(2):57–70.

[Williams and Cieza, 2011] Williams, J. P. and Cieza, L. A. (2011). Protoplanetary disks and their evolution. *Annual Review of Astronomy and Astrophysics*, 49:67–117.

[Wyatt, 2008] Wyatt, M. C. (2008). Evolution of debris disks. *Annu. Rev. Astron. Astrophys.*, 46:339–383.

[Zuckerman et al., 1995] Zuckerman, B., Forveille, T., and Kastner, J. H. (1995). Inhibition of giant-planet formation by rapid gas depletion around young stars. *Nature*, 373(6514):494–496.